optica

Dispersion engineering via nonlocal transformation optics: supplementary material

MASSIMO MOCCIA[1], GIUSEPPE CASTALDI[1], VINCENZO GALDI[1,*], ANDREA ALÙ[2], AND NADER ENGHETA[3]

[1]Waves Group, Department of Engineering, University of Sannio, I-82100, Benevento, Italy
[2]Department of Electrical and Computer Engineering, The University of Texas at Austin, Austin, TX 78712, USA
[3]Department of Electrical and Systems Engineering, University of Pennsylvania, Philadelphia, PA 19104, USA
[*]Corresponding author: vgaldi@unisannio.it

Published 12 February 2016

This document provides supplementary information to "Dispersion engineering via nonlocal transformation optics," http://dx.doi.org/10/1364/optica.3.000179. We give further details on the technical derivations, as well as additional numerical results. Newly introduced equations and figures are labeled with the prefix "S"; all others pertain to the main text. All references are intended as local, and those already utilized in the main text are repeated.

http://dx.doi.org/10.1364/optica.3.000179.s001

1. DETAILS ON NLTO APPROACH

A. Derivation of Eqs. (3) and (4)

We start considering the Maxwell's curl equations pertaining to the auxiliary vacuum space (Fig. 1, left panel),

$$\nabla' \times \mathbf{E}'(\mathbf{r}',\omega) = i\omega\mu_0 \mathbf{H}'(\mathbf{r}',\omega) - \mathbf{M}'(\mathbf{r}',\omega), \tag{S1a}$$
$$\nabla' \times \mathbf{H}'(\mathbf{r}',\omega) = -i\omega\varepsilon_0 \mathbf{E}'(\mathbf{r}',\omega) + \mathbf{J}'(\mathbf{r}',\omega), \tag{S1b}$$

which, via the spatial Fourier transform (1), can be fully algebrized in the auxiliary reciprocal space ($\mathbf{k}'$), viz.,

$$i\mathbf{k}' \times \tilde{\mathbf{E}}'(\mathbf{k}',\omega) = i\omega\mu_0 \tilde{\mathbf{H}}'(\mathbf{k}',\omega) - \tilde{\mathbf{M}}'(\mathbf{k}',\omega), \tag{S2a}$$
$$i\mathbf{k}' \times \tilde{\mathbf{H}}'(\mathbf{k}',\omega) = -i\omega\varepsilon_0 \tilde{\mathbf{E}}'(\mathbf{k}',\omega) + \tilde{\mathbf{J}}'(\mathbf{k}',\omega). \tag{S2b}$$

By applying the phase-space mapping (2), and exploiting the form-invariance properties, Eqs. (S2) can be straightforwardly recast in the form

$$i\mathbf{k} \times \tilde{\mathbf{E}}(\mathbf{k},\omega) = i\omega\mu_0 \underline{\underline{\tilde{\mu}}}(\mathbf{k},\omega) \cdot \tilde{\mathbf{H}}(\mathbf{k},\omega) - \tilde{\mathbf{M}}(\mathbf{k},\omega), \tag{S3a}$$
$$i\mathbf{k} \times \tilde{\mathbf{H}}(\mathbf{k},\omega) = -i\omega\varepsilon_0 \underline{\underline{\tilde{\varepsilon}}}(\mathbf{k},\omega) \cdot \tilde{\mathbf{E}}(\mathbf{k},\omega) + \tilde{\mathbf{J}}(\mathbf{k},\omega), \tag{S3b}$$

where the transformed fields ($\tilde{\mathbf{E}}$, $\tilde{\mathbf{H}}$) and sources ($\tilde{\mathbf{J}}$, $\tilde{\mathbf{M}}$) are given by (3), and the relative permittivity and permeability tensors ($\underline{\underline{\tilde{\varepsilon}}}$, $\underline{\underline{\tilde{\mu}}}$) are given by (4).

B. Physical Restrictions on Transformation Media

As mentioned in the main text, there are some restrictions in the structure of the nonlocal constitutive tensors (4), dictated by basic physical-feasibility properties [1, 2]. For simplicity of illustration, we briefly review these general properties considering the relative permittivity tensor $\underline{\underline{\tilde{\varepsilon}}}$ only, although they also hold for the relative permeability tensor $\underline{\underline{\tilde{\mu}}}$.

First, the *real-valued* character of fields in the physical (space-time) domain yields

$$\underline{\underline{\tilde{\varepsilon}}}(\mathbf{k},\omega) = \underline{\underline{\tilde{\varepsilon}}}^*(-\mathbf{k}^*,-\omega^*), \tag{S4}$$

with * denoting complex conjugation. Moreover, *passivity* implies the *positive-definite* character of the anti-Hermitian part

$$\underline{\underline{\tilde{\varepsilon}}}^A(\mathbf{k},\omega) = \frac{1}{2}\left[\underline{\underline{\tilde{\varepsilon}}}(\mathbf{k},\omega) - \underline{\underline{\tilde{\varepsilon}}}^*(\mathbf{k},\omega)\right], \tag{S5}$$

whereas the absence of losses yields the Hermitian condition

$$\underline{\underline{\tilde{\varepsilon}}}(\mathbf{k},\omega) = \underline{\underline{\tilde{\varepsilon}}}^*(\mathbf{k},\omega). \tag{S6}$$

Also of relevance are the Onsager relations dictated by the space-time symmetry conditions of the dynamical equations in the microscopic model

$$\underline{\underline{\tilde{\varepsilon}}}(\mathbf{k},\omega)\big|_{\mathbf{B}_{ext}} = \underline{\underline{\tilde{\varepsilon}}}^T(-\mathbf{k},\omega)\Big|_{-\mathbf{B}_{ext}}, \tag{S7}$$

with $\mathbf{B}_{ext}$ denoting an external (static) magnetic field induction. In particular, *reciprocity* implies

$$\underline{\underline{\tilde{\xi}}}\left(\mathbf{k},\omega\right)=\underline{\underline{\tilde{\xi}}}^{T}\left(-\mathbf{k},\omega\right) \tag{S8}$$

It can also be shown (see [2] for details) that *stability* and *causality* imply (under generally met regularity conditions) that the constitutive tensors are *analytic* functions in the whole reciprocal space of the complex variable $\mathbf{k}$, and in the upper half ω-plane. This results in Kramers-Kronig-type relations between the Hermitian and anti-Hermitian parts (see [2] for details).

In view of (4), the above relationships translate more or less directly into restrictions on the metric tensor $\underline{\underline{\tilde{\Lambda}}}$, and hence on the coordinate transformation $\tilde{\mathbf{F}}$. In particular, it can be readily verified that a sufficient condition for (S4) is

$$\underline{\underline{\tilde{\Lambda}}}\left(\mathbf{k},\omega\right)=\underline{\underline{\tilde{\Lambda}}}^{*}\left(-\mathbf{k}^{*},-\omega^{*}\right). \tag{S9}$$

Moreover,

$$\underline{\underline{\tilde{\Lambda}}}^{T}\left(\mathbf{k},\omega\right)=\underline{\underline{\tilde{\Lambda}}}^{*}\left(\mathbf{k},\omega\right) \tag{S10}$$

guarantees the Hermitian condition (i.e., absence of losses) in (S6), whereas the *center-symmetry* condition in (6) guarantees reciprocity [cf. (S8)].

Finally, recalling that sums and products of analytic functions are still analytic, it follows from (4) that metric tensors $\underline{\underline{\tilde{\Lambda}}}$ that are *analytic* and *non-singular* in the whole complex k-space and in the upper half ω-plane generally yield transformation media characterized by causal, stable responses.

C. Effectively Nonmagnetic Constitutive Blueprints

It can be observed from (2) that, for a given phase-space mapping $\tilde{\mathbf{F}}\left(\mathbf{k},\omega\right)$, the choice of the associated metric tensor $\underline{\underline{\tilde{\Lambda}}}\left(\mathbf{k},\omega\right)$ is not unique. In view of (3) and (4), different choices of $\underline{\underline{\tilde{\Lambda}}}$ give rise to different field/source effects and transformation media, but they do not affect [in view of (10)] the transformed dispersion law. This is not surprising, as it is well known that different media may exhibit the same dispersion properties.

The degrees of freedom in the choice of $\underline{\underline{\tilde{\Lambda}}}$ can be fruitfully exploited to simplify the structure of the transformation medium and its practical implementation. For instance, for the class of coordinate-separable transformations in (7), a particularly convenient choice is the *diagonal* form

$$\underline{\underline{\tilde{\Lambda}}}\left(k_x,k_z,\omega\right)=\mathrm{diag}\left[\frac{\tilde{F}_x\left(k_x,\omega\right)}{k_x},\frac{\tilde{F}_x\left(k_x,\omega\right)\tilde{F}_z\left(k_z,\omega\right)}{k_xk_z},\frac{\tilde{F}_z\left(k_z,\omega\right)}{k_z}\right] \tag{S11}$$

which yields $\tilde{\mu}_{yy}=1$ in (4). For the assumed transverse-magnetic (TM) polarization, this gives rise to a uniaxially-anisotropic medium with the relevant relative-permittivity components given by (8), and an *effectively nonmagnetic* character which may strongly facilitate implementations at optical frequencies.

2. DETAILS ON MULTILAYERED METAMATERIAL SYNTHESIS

A. Geometry

The multilayered metamaterial configuration of interest is schematized in Fig. S1. We consider a rather general supercell composed of J nonmagnetic, lossless material layers characterized by a relative permittivity tensor $\underline{\underline{\varepsilon}}_j$ and thickness d_j, $j=1,...,J$, stacked along the x-direction. With specific relevance to our application examples, these material layers are

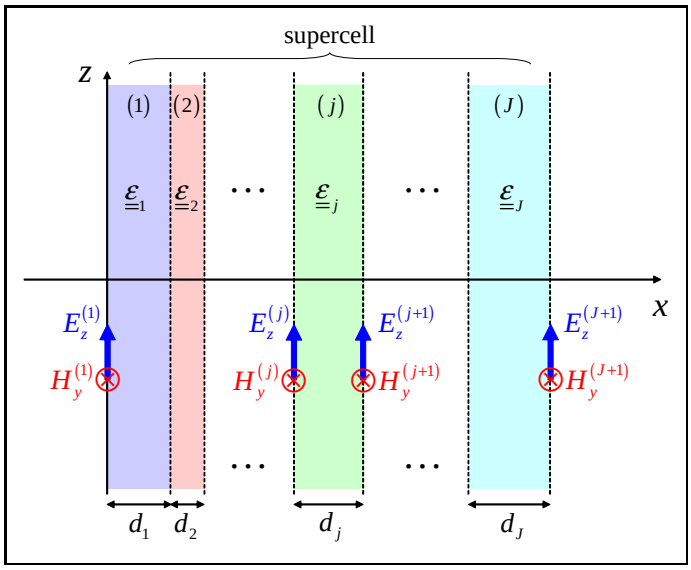

Fig. S1. Schematics of a general metamaterial supercell composed of J nonmagnetic, lossless material layers characterized by relative-permittivity tensors $\underline{\underline{\varepsilon}}_j$ and thicknesses d_j, $j=1,...,J$ stacked along the x-direction. Also shown are the tangential field components $E_z^{(j)}$ and $H_y^{(j)}$ at the layer interfaces, of interest for TM polarization.

either isotropic or gyrotropic [cf. (15)]. Accordingly, in what follows we consider the more general gyrotropic form

$$\underline{\underline{\varepsilon}}_j=\begin{bmatrix}\varepsilon_{dj} & 0 & i\varepsilon_{gj}\\ 0 & 1 & 0\\ -i\varepsilon_{gj} & 0 & \varepsilon_{dj}\end{bmatrix}, \tag{S12}$$

which reduces to the isotropic case for $\varepsilon_{gj}=0$.

B. Exact Dispersion Equation

The dispersion relationship of a multilayered metamaterial obtained via infinite replication of the supercell in Fig. S1 can be rigorously calculated via the well-known transfer-matrix approach [3]. In essence, the relevant tangential field components at the supercell interfaces $x=0$ and $x=d\equiv\sum_{j=1}^{J}d_j$ can be related via a *transfer matrix*,

$$\begin{bmatrix}E_z^{(1)}\\ \eta_0H_y^{(1)}\end{bmatrix}=\underline{\underline{M}}\left(k_z,\omega;\underline{\alpha}\right)\cdot\begin{bmatrix}E_z^{(J+1)}\\ \eta_0H_y^{(J+1)}\end{bmatrix}, \tag{S13}$$

where the (x,z) dependence in the fields has been omitted for notational compactness, η_0 denotes the vacuum characteristic impedance, k_z is the (conserved) transverse wavenumber, and the array $\underline{\alpha}\equiv\left[\underline{\alpha}^{(1)},...,\underline{\alpha}^{(J)}\right]$ contains the constitutive and geometrical parameters of the various layers. The transfer matrix

$$\underline{\underline{M}}\left(k_z,\omega;\underline{\alpha}\right)=\prod_{j=1}^{J}\underline{\underline{M}}^{(j)}\left(k_z,\omega;\underline{\alpha}^{(j)}\right) \tag{S14}$$

is *unimodular* (in view of the assumed absence of losses), and can obtained by cascading the transfer matrices $\underline{\underline{M}}^{(j)}$ associated

with the individual layers, viz.

$$\begin{bmatrix} E_z^{(j)} \\ \eta_0 H_y^{(j)} \end{bmatrix} = \underline{\underline{M}}^{(j)}\left(k_z,\omega;\underline{\alpha}^{(j)}\right)\cdot\begin{bmatrix} E_z^{(j+1)} \\ \eta_0 H_y^{(j+1)} \end{bmatrix}. \quad \textbf{(S15)}$$

In particular, for the gyrotropic material in (S12), we obtain

$$\underline{\underline{M}}^{(j)}\left(k_z,\omega;\underline{\alpha}^{(j)}\right) = \begin{bmatrix} M_{11}^{(j)} & M_{12}^{(j)} \\ M_{21}^{(j)} & M_{22}^{(j)} \end{bmatrix}, \quad \textbf{(S16)}$$

with

$$M_{11}^{(j)} = \cos\delta_j - \frac{\varepsilon_{gj}k_z\sin\delta_j}{\varepsilon_{dj}k_{xj}}, \quad \textbf{(S17a)}$$

$$M_{12}^{(j)} = \frac{i\left(\varepsilon_{dj}^2k_{xj}^2+\varepsilon_{gj}^2k_z^2\right)\sin\delta_j}{\varepsilon_{dj}k_0k_{xj}\left(\varepsilon_{dj}^2-\varepsilon_{gj}^2\right)}, \quad \textbf{(S17b)}$$

$$M_{21}^{(j)} = \frac{ik_0\left(\varepsilon_{dj}^2-\varepsilon_{gj}^2\right)\sin\delta_j}{\varepsilon_{dj}}, \quad \textbf{(S17c)}$$

$$M_{22}^{(j)} = \cos\delta_j + \frac{\varepsilon_{gj}k_z\sin\delta_j}{\varepsilon_{dj}k_{xj}}, \quad \textbf{(S17d)}$$

and

$$\delta_j = k_{xj}d_j,\quad k_{xj} = \sqrt{\frac{k_0^2\left(\varepsilon_{dj}^2-\varepsilon_{gj}^2\right)-k_z^2\varepsilon_{dj}}{\varepsilon_{dj}}},\ \mathrm{Im}\left(k_{xj}\right)\geq 0. \quad \textbf{(S18)}$$

The assumed periodicity along the x-direction dictates Bloch-type phase-shift conditions for the fields at the supercell interfaces $x=0$ and $x=d$, viz.,

$$\begin{bmatrix} E_z^{(1)} \\ \eta_0 H_y^{(1)} \end{bmatrix} = \exp\left(-ik_xd\right)\begin{bmatrix} E_z^{(J+1)} \\ \eta_0 H_y^{(J+1)} \end{bmatrix}, \quad \textbf{(S19)}$$

which, enforced in (S14), yields a homogeneous linear system of equations

$$\left[\underline{\underline{M}}\left(k_z,\omega;\underline{\alpha}\right)-\exp\left(-ik_xd\right)\underline{\underline{I}}\right]\cdot\begin{bmatrix} E_z^{(J+1)} \\ \eta_0 H_y^{(J+1)} \end{bmatrix} = 0, \quad \textbf{(S20)}$$

with $\underline{\underline{I}}$ denoting the 2×2 identity matrix. By enforcing nontrivial solutions of (S20) (i.e., zeroing the matrix determinant) and exploiting the unimodular character of the transfer matrix, we finally obtain the dispersion relationship

$$2\cos\left(k_xd\right) = \mathrm{Tr}\left[\underline{\underline{M}}\left(k_z,\omega;\underline{\alpha}\right)\right], \quad \textbf{(S21)}$$

where Tr denotes the *trace* operator [4].

C. Nonlocal Effective Model

As mentioned in the main text, several nonlocal-homogenization approaches have been proposed for multilayered metamaterials (see, e.g., [5–10]). As in [11], our approach relies on a suitable modification of the framework proposed in [5]. The basic idea is to find a nonlocal uniaxial effective medium whose dispersion relationship

$$\frac{k_x^2}{\tilde{\varepsilon}_{zz}^{(eff)}\left(k_x,\omega;\underline{\alpha}\right)}+\frac{k_z^2}{\tilde{\varepsilon}_{xx}^{(eff)}\left(k_z,\omega;\underline{\alpha}\right)} = \frac{\omega^2}{c^2}, \quad \textbf{(S22)}$$

matches the Taylor expansion of (S21) up to a given order in the arguments within a phase-space region of interest. In our chosen application examples, we are mainly interested in a neighborhood of the phase-space point $k_x=0, k_z=k_{z0}, \omega=\omega_0$.

Accordingly, we begin by expanding both sides of (S21) in Taylor series with respect to k_xd (around $k_x=0$), and with respect to k_z (around k_{z0}) and ω (around ω_0). The result can be conveniently recast as

$$2+2\sum_{n=1}^{N}\frac{(-1)^n}{n!}k_x^{2n}d^{2n} \approx \sum_{m=0}^{M}\sum_{l=0}^{L}\omega^{2m}k_z^ld^{2m+l}\chi_{ml}\left(\underline{\alpha}\right), \quad \textbf{(S23)}$$

with $2N=2M+L$, and χ_{ml} denoting functions of the constitutive and geometrical parameters of the multilayer (with the dependence on k_{z0} and ω_0 omitted for notational compactness). These functions can be calculated analytically via symbolic manipulation tools (in our studies, we utilized Mathematica^{TM} [12]). By factoring out the $l=0$ term, and isolating the k_x- and k_z-dependent terms, (S23) can be recast as

$$\frac{2\sum_{n=1}^{N}\frac{(-1)^{n-1}}{n!}k_x^{2n}d^{2n}}{2-\sum_{m=0}^{M}\omega^{2m}d^{2m}\chi_{m0}\left(\underline{\alpha}\right)}+\frac{\sum_{m=0}^{M}\sum_{l=1}^{L}\omega^{2m}k_z^ld^{2m+l}\chi_{ml}\left(\underline{\alpha}\right)}{2-\sum_{m=0}^{M}\omega^{2m}d^{2m}\chi_{m0}\left(\underline{\alpha}\right)} \approx 1, \quad \textbf{(S24)}$$

which is formally analogous to (S22) if we let

$$\tilde{\varepsilon}_{xx}^{(eff)}(k_z,\omega;\underline{\alpha}) = \frac{c^2\left[2-\sum_{m=0}^{M}\omega^{2m}d^{2m}\chi_{m0}\left(\underline{\alpha}\right)\right]}{\sum_{m=0}^{M}\sum_{l=1}^{L}\omega^{2(m+1)}k_z^{l-2}d^{2m+l}\chi_{ml}(\underline{\alpha})}, \quad \textbf{(S25a)}$$

$$\tilde{\varepsilon}_{zz}^{(eff)}(k_x,\omega;\underline{\alpha}) = \frac{c^2\left[2-\sum_{m=0}^{M}\omega^{2m}d^{2m}\chi_{m0}\left(\underline{\alpha}\right)\right]}{2\omega^2\sum_{n=1}^{N}\frac{(-1)^{n-1}}{n!}k_x^{2(n-1)}d^{2n}}. \quad \textbf{(S25b)}$$

The expressions in (S25) therefore constitute the sought nonlocal effective parameters. We observe that they exhibit a *rational* structure which, over suitably limited regions of the $(\mathbf{k},\omega)$ phase space, may approximately match that of the NLTO blueprints in (8), with a reasonably limited number of terms (see Section 3 below for details pertaining to the specific examples)

D. Parameter Optimization

As illustrated in the main text, the metamaterial synthesis problem can be posed as a parameter optimization enforcing a reasonable matching between the desired NLTO blueprints and the nonlocal effective model. In fact, the parameter-optimization problem may be relaxed by exploiting possible degrees of freedom in the NLTO blueprints. Accordingly, by symbolically grouping such degrees of freedom in a parameter-array $\underline{\beta}$, the general parameter-optimization problem in (5) can be reformulated as

$$\left[\underline{\alpha}^{(opt)},\underline{\beta}^{(opt)}\right] = \underset{\underline{\alpha},\underline{\beta}}{\mathrm{argmin}}\Big\{\left\|\tilde{\varepsilon}_{xx}^{(TO)}\left(k_z,\omega;\underline{\beta}\right)-\tilde{\varepsilon}_{xx}^{(eff)}(k_z,\omega;\underline{\alpha})\right\|_S^2 + \left\|\tilde{\varepsilon}_{zz}^{(TO)}\left(k_x,\omega;\underline{\beta}\right)-\tilde{\varepsilon}_{zz}^{(eff)}\left(k_x,\omega;\underline{\alpha}\right)\right\|_S^2\Big\}, \quad \textbf{(S26)}$$

with the choice of the error metrics and region S of the $(\mathbf{k},\omega)$ phase space depending on the specific application (see Section 3 below for details pertaining to the various examples).

The minimization of the error functional in (S26) is performed via an approach similar to that utilized in [13]. More specifically, we utilize a combination of the Nelder-Meald (simplex) and differential-evolution unconstrained optimization algorithms implemented in the Mathematica^{TM} `NMinimize` function [12]. Given the highly nonlinear character of the optimization problem, and the consequent presence of many local minima (i.e., false solutions), we implemented a synthesis strategy based on randomly moving the initial guess across a reasonable parameter range, so as to explore different regions of the search-space. Within this framework, required constraints on the NLTO parameters [e.g., (14)] and/or the constitutive/geometrical parameters of the multilayer (in order to guarantee the practical feasibility) are enforced in a *soft* fashion via the choice of initial-guess parameter ranges, and verified *a posteriori* by discarding candidate solutions that fall outside these ranges. While not guaranteeing a convergence to the global minimum, we found that this strategy strongly mitigates the dependence on the initial guess, and typically allows to attain satisfactorily low levels of the error functional.

3. DETAILS ON APPLICATION EXAMPLES

A. One-Way Propagation

As illustrated in the main text, the problem can be mathematically formulated by requiring that the transformed dispersion equation for $k_x = 0$ and $\omega = \omega_0$,

$$\frac{\omega_0^2 \tilde{Q}(k_z)}{W^2(\omega_0)} = k_0^2, \tag{S27}$$

admits only one positive solution $k_z = k_{z0} > 0$. The possibly simplest choice for the transformation is therefore a frequency-independent, non-centrosymmetric mapping with $W(\omega) = \omega$ and a *cubic* k_z-dependence,

$$\tilde{Q}(k_z) = (k_z - k_{z0})\left(q_0 + q_1 k_z + q_2 k_z^2\right) + k_0^2, \tag{S28}$$

where the fulfillment of (S27) for $k_z = k_{z0}$ has already been enforced. Moreover, it is expedient to choose

$$q_0 = \frac{k_0^2}{k_{z0}^2}, \tag{S29}$$

so that NLTO-blueprint $\tilde{\varepsilon}_{xx}$ in (8) vanishes *linearly* as $k_z \to 0$, in order to structurally match the behavior of the nonlocal effective model in (S25a). The constraint on the q_1 and q_2 parameters in (14) readily follows by enforcing that the quadratic polynomial in (S28) does not admit real roots (negative discriminant), so that $k_z = k_{z0}$ is indeed the only solution of the transformed dispersion equation (S27).

Within a neighborhood of the nominal design point ($k_x \approx 0$, $k_z \approx k_{z0}$, $\omega = \omega_0$), the nonlocal effective constitutive parameters can be accurately represented by truncating the series in (S25) to $M = 0$, $N = 2$, and $L = 3$. Moreover, for the assumed *frequency-independent* transformation, the particular choice in (12) yields a *constant* value of $\tilde{\varepsilon}_{zz}^{(TO)}$. For this component, it appears expedient to enforce the parameter-matching *analytically*, via

$$\begin{aligned} p_2 &= \frac{1}{\tilde{\varepsilon}_{zz}^{(TO)}\left(k_x = 0, \omega_0; \underline{\beta}\right)} \\ &= \frac{1}{\tilde{\varepsilon}_{zz}^{(eff)}\left(k_x = 0, \omega_0; \underline{\alpha}\right)} \approx \frac{2\omega_0^2 d^2}{c^2\left[2 - \chi_{00}\left(\underline{\alpha}\right)\right]}, \end{aligned} \tag{S30}$$

and remove the corresponding term in (S26). The remaining term is defined as a weighted square error

$$\begin{aligned} &\|\tilde{\varepsilon}_{xx}^{(TO)}\left(k_z, \omega; \underline{\beta}\right) - \tilde{\varepsilon}_{xx}^{(eff)}(k_z, \omega; \underline{\alpha})\|_S^2 = \\ &\sum_{j=1}^{J} w_j \left|\tilde{\varepsilon}_{xx}^{(TO)}\left(k_{zj}, \omega_0; \underline{\beta}\right) - \tilde{\varepsilon}_{xx}^{(eff)}\left(k_{zj}, \omega_0; \underline{\alpha}\right)\right|^2, \end{aligned} \tag{S31}$$

with w_j and k_{zj}, $j = 1, ..., J$ denoting positive weight coefficients and discrete k_z-samples, respectively, and the array $\underline{\beta}$ including the TO parameters p_2 [chosen according to (S30)], q_1 and q_2 [subject to (14)]. In principle, the parameter matching should be enforced over the entire k_z range. In practice, we chose $J = 50$ samples equispaced within a suitably broad range $-6k_0 \le k_z \le 6k_0$, with larger weights ($w_j = 4$) assigned to sample points k_{zj} falling within a 10% neighborhood of $k_{z0} = 4.5k_0$, where the design prescriptions are stricter and the nonlocal effective model is also more accurate. In the rest of the k_z-range, where a looser prescription of evanescent behavior applies and the nonlocal effective model is less accurate, the synthesis is relaxed by choosing smaller weights ($w_j = 1$).

For the optimized configuration, Fig. S2 compares the EFCs obtained via the nonlocal effective model and those obtained by numerically solving the exact dispersion equation of the multilayered metamaterial. A generally good agreement is observed, especially around the nominal design point. Overall, the nonlocal effective model captures the essential dispersion features (in particular, the one-way character) over a fairly broad parameter range.

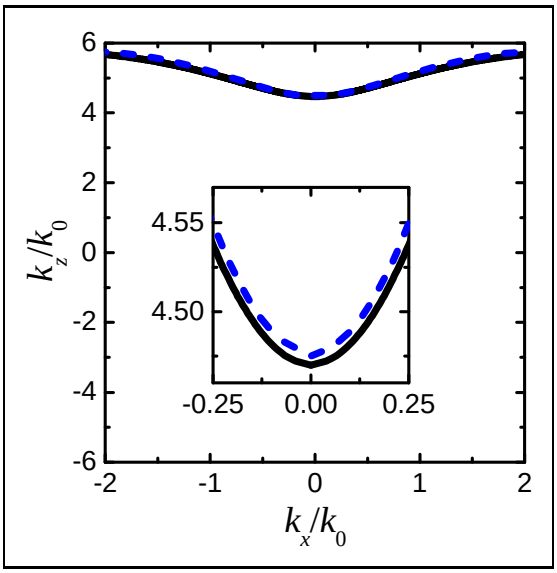

Fig. S2. As in Fig. 3(c), but comparison between the EFCs computed via the nonlocal effective parameters (S25) (with $M = 0$, $N = 2$, $L = 3$; blue-dashed curves) and by numerically solving the exact dispersion equation of the synthesized metamaterial (black-solid curves).

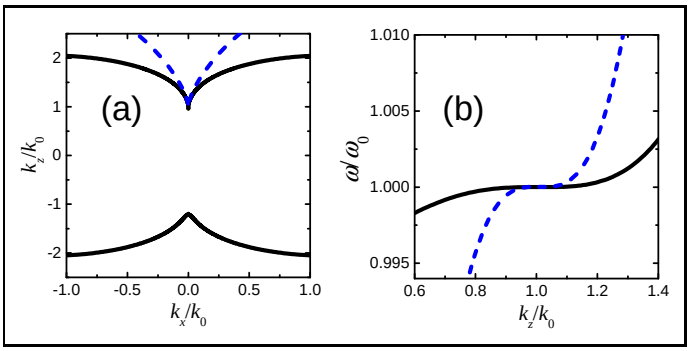

Fig. S3. (a), (b) As in Figs. 4(c) and 4(d), but comparisons between the EFCs and dispersion diagrams, respectively, computed via the nonlocal effective parameters (S25) (with $M = 0$, $N = 2$, $L = 3$; blue-dashed curves) and by numerically solving the exact dispersion equation of the synthesized metamaterial (black-solid curves).

As pointed out in the main text, although no particular emphasis on the technological feasibility was placed in this prototype study, attention was paid so as to constrain the constitutive parameters of the material constituents within realistic bounds. For instance, the parameters of the gyrotropic material in (15) are compatible with certain configurations of magnetically-biased graphene considered in the literature (see, e.g., [14]).

B. Stationary Points in the Dispersion Relationship

Although the tailoring of a stationary point in the (ω, k_z) dispersion diagram may seem to inherently require a *frequency-dependent* transformation, simple considerations show that this is not the case. By solving the transformed dispersion equation with respect to ω, we obtain

$$\omega = c\sqrt{\tilde{P}(k_x) + \tilde{Q}(k_z)}, \tag{S32}$$

from which it readily follows that

$$\frac{\partial^n \omega}{\partial (k_z)^n} \propto \frac{\partial^n \tilde{Q}(k_z)}{\partial (k_z)^n}. \tag{S33}$$

In other words, the stationary-point condition (16) can be equivalently enforced in $\tilde{Q}$, without the need of a frequency-dependent transformation. We can therefore choose $W(\omega) = \omega$ and

$$\tilde{Q}(k_z) = q_N (k_z - k_{z0})^N + \tilde{R}(k_z) + k_0^2, \tag{S34}$$

with

$$\tilde{R}(k_z) = \sum_{n>N} r_n (k_z - k_{z0})^n, \tag{S35}$$

with r_n denoting constant coefficients. The expression in (17) corresponds to the possibly simplest choice $\tilde{R} = 0$.

For the synthesis procedure, similar considerations as in the previous example hold. Also in this case, we truncate the series in (S25) to $M = 0$, $N = 2$, $L = 3$ and, in view of the frequency-independent character of the transformation, we exploit (S30) and (S31). However, unlike the previous example, the parameter matching can now be enforced within a small neighborhood of the nominal design point. Accordingly, we consider in (S31) $J = 5$ samples equispaced within the interval $0.9k_0 \le k_z \le 1.1k_0$, with identical weights. Also in this case, the nonlocal effective model accurately captures the dispersion effects around the nominal design point, as shown by the comparison in Fig. S3 with the actual synthesis results. Similar considerations as for the previous example also hold in connection with the realistic bounds enforced on the material-constituent parameters.

C. Dirac-Point Conical Singularities

To derive a centrosymmetric approximant of the dispersion relationship in (18) in the vicinity of the Dirac-point conical singularity, we recall that for $k_z \approx k_{z0}$ and $\omega \approx \omega_0$

$$k_z - k_{z0} \approx \frac{k_z^2 - k_{z0}^2}{2k_{z0}}, \quad \omega - \omega_0 \approx \frac{\omega^2 - \omega_0^2}{2\omega_0}. \tag{S36}$$

Application of these approximations in (18) yields

$$\gamma_x k_x^2 + \gamma_z \frac{\left(k_z^2 - k_{z0}^2\right)^2}{4k_{z0}^2} \approx \frac{\left(\omega^2 - \omega_0^2\right)^2}{4c^2\omega_0^2}, \tag{S37}$$

from which the expressions in (20) readily follow via simple algebra.

The metamaterials synthesis procedure in this example differs from the previous two cases, in view of the frequency-dependent character of the underlying transformation. In particular, the series in (S25) are truncated to $M = N = L = 2$, so as to include the explicit temporal dispersion. Moreover, we can no longer rely on the analytical parameter matching (S30), and should therefore consider the full optimization problem (S26) over a suitable region of the $(\mathbf{k}, \omega)$ phase space. In our procedure, we considered standard square-error metrics

$$\|\tilde{\varepsilon}_{xx}^{(TO)}\left(k_z, \omega; \underline{\beta}\right) - \tilde{\varepsilon}_{xx}^{(eff)}(k_z, \omega; \underline{\alpha})\|_S^2 = \sum_{j=1}^{J} \left|\tilde{\varepsilon}_{xx}^{(TO)}\left(k_{zj}, \omega_j; \underline{\beta}\right) - \tilde{\varepsilon}_{xx}^{(eff)}\left(k_{zj}, \omega_j; \underline{\alpha}\right)\right|^2, \tag{S38}$$

$$\|\tilde{\varepsilon}_{zz}^{(TO)}\left(k_x, \omega; \underline{\beta}\right) - \tilde{\varepsilon}_{zz}^{(eff)}(k_x, \omega; \underline{\alpha})\|_S^2 = \sum_{j=1}^{J} \left|\tilde{\varepsilon}_{zz}^{(TO)}\left(k_{xj}, \omega_j; \underline{\beta}\right) - \tilde{\varepsilon}_{zz}^{(eff)}\left(k_{xj}, \omega_j; \underline{\alpha}\right)\right|^2, \tag{S39}$$

with the array $\underline{\beta}$ including the TO parameters γ_z and k_{z0}, and ω_j, k_{xj} and k_{zj}, $j = 1, ..., J$ denoting phase-space sample points in a small neighborhood of the nominal Dirac points. More specifically, we considered $J = 5$ radian-frequency samples ω_j equispaced within the interval $0.995\omega_0 \le \omega \le 1.005\omega_0$, and derived the corresponding k_{xj} and k_{zj} samples from the ideal conical dispersion relationship (18) in the two principal planes, viz.,

$$k_{xj} = \pm\frac{\omega_j - \omega_0}{c\sqrt{\gamma_x}}, \quad k_{zj} = k_{z0} \pm \frac{\omega_j - \omega_0}{c\sqrt{\gamma_z}}, \quad j = 1, ..., J. \tag{S40}$$

From the comparison shown in Fig. S4, we observe that also in this case the nonlocal effective parameters capture the dispersion characteristics of the actual synthesized metamaterial, with a fairly good agreement in the $k_z = k_{z0}$ plane, and a slightly worse approximation in the $k_x = 0$ plane.

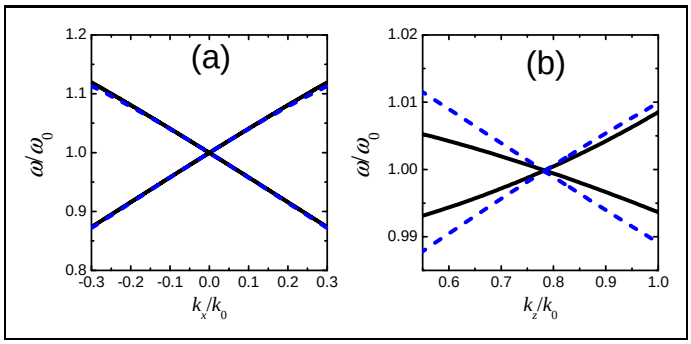

Fig. S4. (a), (b) As in Figs. 5(c) and 5(d), respectively, but comparisons between the dispersion diagrams (for $k_z = k_{z0}$ and $k_x = 0$, respectively) computed via the nonlocal effective parameters (S25) (with $M = N = L = 2$; blue-dashed curves) and by numerically solving the exact dispersion equation of the synthesized metamaterial (black-solid curves).

4. DETAILS ON NUMERICAL SIMULATIONS

In all examples, the EFCs and dispersion diagrams pertaining to the synthesized multilayered metamaterials are computed by numerically solving the exact dispersion equation (S21) by means of the Mathematica^{TM} `NSolve` function [12].

The field maps and related quantities are computed via the finite-element-based commercial software COMSOL Multiphysics [15]. In all examples, the MUMPS direct solver is utilized, with default parameters.

More specifically, in the one-way-propagation example (Fig. 3), the computational domain is composed of a single supercell of total length $6\lambda_0$ along the z-direction and periodic boundary conditions along the x-direction. In order to simulate an infinite structure, a $60\lambda_0$-long lossy section of the supercell (with a linearly-increasing loss profile) is added at each side. The computational domain is discretized with a maximum mesh size of $\lambda_0/200$, resulting into about 17.3 million degrees of freedom.

In the frozen-mode example (Fig. 4), a single supercell is considered, with length $10\lambda_0$ along the z-direction and periodic boundary conditions along the x-direction. Also in this case, a $60\lambda_0$-long lossy section of the supercell (with a linearly-increasing loss profile) is added at one side in order to simulate a semi-infinite structure. The other side is terminated by a $2\lambda_0$-long section of vacuum from which the plane-wave illumination impinges. A maximum mesh size of $\lambda_0/100$ is utilized, resulting into about 5.5 million degrees of freedom.

Finally, in the Dirac-point example (Fig. 5), a finite-size structure composed of 200 supercells is considered, with length of $2\lambda_0$ along the z-direction and perfectly-matched-layers terminations along the x-direction. Once again, a lossy section of the structure (with a linearly-increasing loss profile) is added at one side in order to simulate a semi-infinite structure, while the other side is terminated by $3\lambda_0$-long section of vacuum from which the Gaussian-beam-illumination impinges. In this case, a maximum mesh size of $\lambda_0/25$ is utilized, resulting into about 18.8 million degrees of freedom.

REFERENCES

1. L. D. Landau, J. S. Bell, J. Kearsley, Pitaevskii, L.P., E. M. Lifshitz, and J. B. Sykes, *Electrodynamics of Continuous Media, vol. 8*, Course of Theoretical Physics (Elsevier Science, 1984).
2. V. M. Agranovich and V. Ginzburg, *Crystal Optics with Spatial Dispersion, and Excitons*, Springer Series in Solid-State Sciences (Springer, 2013).
3. M. Born and E. Wolf, *Principles of Optics, 7th Ed.* (Cambridge University Press, Cambridge, UK, 1999).
4. S. Lang, *Linear Algebra, 3rd Ed.* (Springer, Berlin, 1987).
5. J. Elser, V. A. Podolskiy, I. Salakhutdinov, and I. Avrutsky, "Nonlocal effects in effective-medium response of nanolayered metamaterials," Appl. Phys. Lett. **90**, 191109 (2007).
6. A. V. Chebykin, A. A. Orlov, A. V. Vozianova, S. I. Maslovski, Y. S. Kivshar, and P. A. Belov, "Nonlocal effective medium model for multilayered metal-dielectric metamaterials," Phys. Rev. B **84**, 115438 (2011).
7. A. V. Chebykin, A. A. Orlov, C. R. Simovski, Y. S. Kivshar, and P. A. Belov, "Nonlocal effective parameters of multilayered metal-dielectric metamaterials," Phys. Rev. B **86**, 115420 (2012).
8. R.-L. Chern, "Spatial dispersion and nonlocal effective permittivity for periodic layered metamaterials," Opt. Express **21**, 16514–16527 (2013).
9. A. Ciattoni and C. Rizza, "Nonlocal homogenization theory in metamaterials: Effective electromagnetic spatial dispersion and artificial chirality," Phys. Rev. B **91**, 184207 (2015).
10. L. Sun, Z. Li, T. S. Luk, X. Yang, and J. Gao, "Nonlocal effective medium analysis in symmetric metal-dielectric multilayer metamaterials," Phys. Rev. B **91**, 195147 (2015).
11. G. Castaldi, V. Galdi, A. Alù, and N. Engheta, "Nonlocal transformation optics," Phys. Rev. Lett. **108**, 063902 (2012).
12. Wolfram Research, Inc., *Mathematica Version 10.2* (Wolfram, Champaign, IL, 2015).
13. A. Silva, F. Monticone, G. Castaldi, V. Galdi, A. Alù, and N. Engheta, "Performing mathematical operations with metamaterials," Science **343**, 160–163 (2014).
14. X. Lin, Y. Xu, B. Zhang, R. Hao, H. Chen, and E. Li, "Unidirectional surface plasmons in nonreciprocal graphene," New J. Phys, **15**, 113003 (2013).
15. COMSOL Group, *COMSOL Multiphysics: Version 5.0* (COMSOL, Stockholm, 2015).